Multicellular spheroid based on a triple co-culture: A novel 3D model to mimic pancreatic tumor complexity.

Gianpiero Lazzari, Valérie Nicolas, Michiya Matsusaki, Mitsuru Akashi, Patrick Couvreur, Simona Mura

Multicellular spheroid based on a triple co-culture: a novel 3D model to mimic pancreatic tumor complexity

Gianpiero Lazzari[a], Valerie Nicolas [b], Michiya Matsusaki [c,d], Mitsuru Akashi [e], Patrick Couvreur[a,*], Simona Mura[a,*]

[a]Institut Galien Paris-Sud, UMR 8612, CNRS, Univ Paris-Sud, Université Paris-Saclay, Faculté de Pharmacie, 5 rue Jean-Baptiste Clément, F-92296 Châtenay-Malabry cedex, France.

[b]Institut Paris-Saclay d'Innovation Thérapeutique (IPSIT), UMS IPSIT Université Paris-Sud US 31 INSERM, UMS 3679 CNRS, Plate-forme d'imagerie cellulaire, 5 rue Jean-Baptiste Clément, 92296 Châtenay-Malabry cedex, France

[c]Department of Applied Chemistry, Graduate School of Engineering, Osaka University, 2-1 Yamadaoka, Suita, Osaka 565-0871, Japan

[d]JST, PRESTO, 4-1-8 Honcho, Kawaguchi, Saitama, 332-0012, Japan

[e]Department of Frontier Biosciences, Osaka University Graduate School of Frontier Biosciences, 1-3 Yamadaoka, Suita, Osaka 565-0871, Japan

*****Corresponding author.

E-mail address: simona.mura@u-psud.fr; patrick.couvreur@u-psud.fr

Abstract

The preclinical drug screening of pancreatic cancer treatments suffers from the absence of appropriate models capable to reproduce *in vitro* the heterogeneous tumor microenvironment and its stiff desmoplasia. Driven by this pressing need, we describe in this paper the conception and the characterization of a novel 3D tumor model consisting of a triple co-culture of pancreatic cancer cells (PANC-1), fibroblasts (MRC-5) and endothelial cells (HUVEC), which assembled to form a hetero-type multicellular tumor spheroid (MCTS). By histological analyses and Selective Plain Illumination Microscopy (SPIM) we have monitored the spatial distribution of each cell type and the evolution of the spheroid composition. Results revealed the presence of a core rich in fibroblasts and fibronectin in which endothelial cells were homogeneously distributed. The integration of the three cell types enabled to reproduce *in vitro* with fidelity the influence of the surrounding environment on the sensitivity of cancer cells to chemotherapy. To our knowledge, this is the first time that a scaffold-free pancreatic cancer spheroid model combining both tumor and multiple stromal components has been designed. It holds the possibility to become an advantageous tool for a pertinent assessment of the efficacy of various therapeutic strategies.

Keywords

Multicellular tumor spheroids; pancreatic cancer; 3D models; tumor microenvironment; layer-by-layer coating

1. Introduction

In vitro models capable to faithfully mimic the complex cancer physiopathology represent an unmet need to improve the significance of preclinical research data in the early phase of drug development. It is well known that the tumor biology results from a mutual interaction between cancer cells and the surrounding microenvironment [1]. For instance, extracellular matrix (ECM) proteins, such as fibronectin (FN), are actively involved in tumor stiffness regulation [2, 3] as well as in promotion of tumor growth [4, 5] and drug resistance [6, 7]. Moreover, the intricate cross-talking between cancer cells and stroma components (*e.g.*, fibroblasts, immune and endothelial cells) regulates different features related to tumor progression [8-10]. Fibroblasts influence both the tumor development and the metastatic potential of cancer cells through direct heterotypic cell-to-cell contacts and paracrine factors [11-14]. Interactions with cancer cells, fibroblasts and ECM proteins are required to allow the migration and the proliferation of endothelial cells during tumor vascularization [15, 16].

Multicellular tumor spheroids (MCTS) are the most widely used 3D *in vitro* model in oncology preclinical research and their power of prediction of the *in vivo* efficacy of various chemotherapeutic agents has been clearly evidenced [17, 18]. MCTS reproduce some important key factors of real tumors such as: *(i)* the formation of nutrients, oxygen and metabolic waste diffusive gradients, (*ii)* the organization of cells in layers with different proliferation rates, (*iii)* the presence of cell-to-cell interactions and signalling, (*iv)* the expression of specific gene patterns and (*v)* the chemoresistance [19, 20]. Still, conventional MCTS consisting exclusively of cancer cells mimic only partially the real tumors as consequence of an insufficient extracellular matrix deposition and the absence of other cell types, which compose the tumor microenvironment. With the aim to overcome these limitations hetero-type MCTS consisting of 3D co-cultures of cancer cells and stroma cells have been proposed [21-24]. In addition, the embedding of mono- and hetero-type MCTS in exogenous 3D matrices has been extensively

used, creating a cell-supportive environment and reproducing the cell-to-matrix interactions [25, 26]. Undoubtedly, the use of matrices, such as natural hydrogels (Matrigel® and collagen I, mainly) or synthetic polymers (*e.g.*, poly(ethylene glycol), poly(lactide-*co*-glycolide) and poly(N-isopropylacrylamide)), enhanced the structural stability of 3D MCTS and endowed them with higher biological relevance [27].

However, several disadvantages characterize these approaches. They include: *(i)* the unknown composition of natural hydrogels and the batch-to-batch variability responsible for a lack of reproducibility [21], *(ii)* the difficulty to harvest single spheroids once embedded in synthetic biomaterials and the need to apply experimental procedures (chemical or physical) often toxic and/or detrimental for the cells [28], *(iii)* the restricted accessibility of embedded spheroids, which often makes time-consuming the set-ups to carry out quantitative measurements [23, 27]. In this context, it is evident that the *in vitro* assessment of the role of the microenvironment on the malignant behaviour of tumors and the response to treatments is still a challenge.

Aiming to face this issue, we describe here a novel hetero-type 3D spheroid model integrating cancer cells together with cellular and acellular stroma components (*i.e.*, fibroblasts, endothelial cells, ECM), focusing our attention on the pancreatic ductal adenocarcinoma (PDAC). PDAC belongs to the first five most lethal type of cancers in the western world and the progress in its treatment remains too slow as a consequence of the complex physiopathology of this tumor characterized by a heterogeneous cellular composition and the accumulation of a very dense fibrotic tissue (*i.e.*, desmoplasia) [29]. In PDAC, the crosstalk between cancer and stroma cells leads to a dramatic increase in FN and collagen deposition [10, 14, 30], which causes the collapse of the tumor vessels and the formation of an aberrant and disorganised vascular network [31]. The consequent oxygen and nutrients deficiency induces the secretion of pro-angiogenic molecules that, in turn, increase the aggressiveness and the invasiveness of cancer cells [31-33]. Currently available hetero-type MCTS of PDAC are better representative of the

pathological condition in comparison with 2D monolayer cultures, however they often lack an accurate characterization [34, 35] or consist of no more than two cell types [36-41]. For instance, MCTS made of cancer cells and fibroblasts have been proposed to mimic *in vitro* the molecular cross-talk which characterize the PDAC desmoplasia [36-38, 40, 41]. Similarly, cancer and endothelial cells were assembled in MCTS to reproduce the tumor angiogenesis and its influence on cancer cell invasiveness [39]. However, to the best of our knowledge, hetero-type pancreatic tumor spheroids including fibroblasts and endothelial cells, both essential components of the PDAC microenvironment, have not been previously reported. This was likely due to the difficulty to find the experimental conditions required to obtain viable three-cell-type PDAC multicellular spheroids. In this context, we herein report on the step-by-step construction and detailed characterization of a scaffold-free multicellular tumor spheroid consisting of a triple co-culture of pancreatic cancer cells (PANC-1), fibroblasts (MRC-5) and endothelial cells (HUVEC). Importantly, we demonstrated that the presence of a complex microenvironment reduced the sensitivity of cancer cells to chemotherapy thus closely mimicking the resistance to treatments observed *in vivo*. Overall, this original scaffold-free MCTS represents a pertinent and easy-to-handle tool, which could be readily introduced in routine preclinical screening of therapeutic strategies for pancreatic cancer treatment.

2. Materials and methods

2.1. Cell lines

Human pancreatic cancer cells (PANC-1), human lung fibroblasts (MRC-5) and human umbilical vein endothelial cells (HUVEC) were purchased from ATCC (France) and maintained as recommended. Briefly, PANC-1 cells were maintained in Dulbecco's Modified Eagle Medium-high glucose (DMEM, Sigma Aldrich, France) supplemented with 10% heat-inactivated fetal bovine serum (FBS, Gibco, France). MRC-5 cells were cultured in Eagle's

Minimum Essential Medium (EMEM, Sigma Aldrich, France) supplemented with 10% heat-inactivated FBS and 1% of 200 mM L-Glutamine solution (Sigma Aldrich, France). The luciferase-expressing human pancreatic cell line (BxPC-3-luc2) was obtained from PerkinElmer (Roissy, France) and maintained in Roswell Park Memorial Institute medium (RPMI, Sigma Aldrich, France) supplemented with 10% heat-inactivated FBS. All media were further supplemented with penicillin (50 $U.mL^{-1}$) and streptomycin (0.05 $mg.mL^{-1}$) (Sigma Aldrich, France). HUVEC cells were maintained in endothelial growth medium (EGM-2) consisting of endothelial basal medium (EBM-2) in which supplements and growth factors have been added according to manufacturer instruction (EGM-2 BulletKit Lonza, France). Cells were maintained in a humid atmosphere at 37 °C with 5% CO_2. Cells were used below passage 8 after thawing and harvested at a confluence of 70-80%.

2.2. Cell transfection

Luciferase- and fluorescent protein-expressing cells were created by stable lentiviral transduction according to manufacturer protocols.

For the luciferase-transduction, PANC-1 cells (2.5×10^4 $cells.mL^{-1}$) were seeded in 24-well plates (1 mL/well) and incubated for 24 h in a humid atmosphere at 37 °C with 5% CO_2. Transduction was performed by addition of RediFect™ Red-FLuc-Puromycin lentiviral particles (Perkin-Elmer, France) to cells. For green fluorescent protein (GFP)-transduction, MRC-5 fibroblasts (9×10^4 $cells.mL^{-1}$) were seeded in 24-well plates (1 mL/well) and incubated for 24 h in a humid atmosphere at 37 °C with 5% CO_2. Transduction was performed by addition of pLenti-C-mGFP-P2A-Puro particles (Origene, Germany) to cells. For both cell types, a polybrene (8 $\mu g.mL^{-1}$)-containing medium and a multiplicity of infection (MOI) of 10 were used.

For red fluorescent protein (RFP)-transduction, HUVEC cells (5 x 10^3 cells.mL^{-1}) were seeded in 24-well plates (1 mL/well) and incubated for 24 h in a humid atmosphere at 37 °C with 5% CO_2. Transduction was performed by adding pLenti-C-mRFP-P2A-Puro particles (Origene, Germany) to cells. In this case a MOI 100 in polybrene-free medium was used.

For each experiment, transduction particle-containing medium was removed after 24 h and replaced with fresh medium containing puromycin (Thermo Fisher Scientific, France) as selection antibiotic. According to the specific cell sensitivity, puromycin was used at a concentration of 2, 1 and 0.5 µg.mL^{-1} for PANC-1, MRC-5 and HUVEC cells, respectively. Puromycin-containing medium was replaced every 3 days until resistant colonies could be identified. Cell bioluminescence and fluorescence were measured 48 h after infection and prior to the cryopreservation of selected cells.

2.3. Construction of 3D MCTS

2.3.1. Liquid overlay technique

Mono-type and hetero-type MCTS were constructed according to the liquid overlay technique [42] using 96 round-bottomed well plates (CELLSTAR®, Sigma Aldrich, France). Before use, 50 µL of 1.2 % (w/v) poly-2-hydroxyethyl methacrylate (poly-HEMA, Sigma Aldrich, France) ethanolic solution was added to each well, and solvent was evaporated in sterile conditions.

For the construction of the mono-type PANC-1 spheroids, cell suspensions (2.5, 5, 12.5 or 25 x 10^3 cells.mL^{-1}) were prepared in DMEM complete medium and 200 µL of the cell suspensions (corresponding to 500, 1000, 2500 and 5000 cells, respectively) was transferred into each well. For the construction of the hetero-type PANC-1:MRC-5 spheroids, suspensions of each cell type were prepared in DMEM complete medium and then 200 µL of their opportune mixture

was transferred into each well. The number of PANC-1 cells was fixed at 500 cells per well. Four PANC-1:MRC-5 ratios have been studied (*i.e.*, 1:1; 1:2; 1:4 and 1:9).

For the construction of the hetero-type PANC-1:MRC-5:HUVEC spheroids, suspensions of each cell type were prepared in DMEM complete medium and then 200 µL of their opportune mixture was transferred into each well. The number of PANC-1 was fixed at 500 cells per well. A ratio of 1:9:4 among PANC-1:MRC-5:HUVEC has been studied. Optimization of the experimental protocol included *(i)* construction of a nanofilm of fibronectin-gelatin (FN-G) at the MRC-5 surface before seeding (*see 2.3.2*) and *(ii)* addition of human VEGF (50 $ng.mL^{-1}$) (Thermo Fisher Scientific, France) to the culture medium.

Cell dispersions at different densities were prepared after automatic cell counting (Countess II, Thermo Fisher Scientific, France), according to manufacturer instructions. After cell seeding, plates were centrifuged (1100 rpm, 5 minutes, 20 °C) and then incubated in a humidified atmosphere with 5% CO_2 at 37 °C for a minimum of 48 h. For long term culture, half of the medium was replaced every 3 days.

MCTS constructed with luciferase-expressing cells were prepared according to the same protocols except for the use of phenol red-free DMEM (Sigma Aldrich, France) supplemented with 10% heat-inactivated FBS, 1% of 200 mM L-Glutamine solution, 1% of 100 mM sodium pyruvate solution (Sigma Aldrich, France), penicillin (50 $U.mL^{-1}$) and streptomycin (0.05 $mg.mL^{-1}$). Fluorescently-labelled spheroids were prepared using GFP-expressing MRC-5 fibroblasts and RFP-expressing HUVEC cells.

2.3.2. Fibronectin-gelatin coating of MRC-5

A fibronectin-gelatin nanometer sized film was constructed at the MRC-5 surface according to the previously validated Layer-by-Layer (LbL) method [43]. Briefly, after trypsinization, fibroblasts were suspended in 1 mL of Tris-HCl buffer (50 mM, pH 7.4) (Sigma Aldrich, France), centrifuged (2500 rpm, 1 minute, room temperature) and then alternatively incubated for 1 minute using a Microtube Rotator (VWR, France) in 1 mL of 0.04 $mg.mL^{-1}$ Human fibronectin or gelatin (Sigma Aldrich, France) Tris-HCl solutions (50 mM, pH 7.4). Each incubation was followed by a centrifugation (2500 rpm, 1 minute, room temperature) and a washing step with Tris-HCl buffer (1 mL, 50 mM, pH 7.4). A total of 9 coating steps were performed. Then, fibroblasts were suspended in cell culture medium and used to construct the triple co-culture, as above described.

2.4. Spheroid characterization

2.4.1. Optical imaging

Routine spheroid monitoring was performed using the AxioObserver Z1 (Carl Zeiss, Germany) inverted microscope equipped with a Peltier cooled (- 40 °C) CoolSnap HQ2 CCD camera (Photometrics,Tucson, USA) and a XL incubator thermostated at 37 °C providing 5% CO_2. Transmitted light images of spheroids were collected directly from the poly-HEMA coated plates with a Plan-Apochromat 2.5x dry objective lens, a halogen lamp and a motorized stage used on an automated mode (AxioVision software / high content acquisitions).

By using an image-processing macro, specifically created with the Image-J® software, morphometric parameters such as spheroid area, perimeter, minimum diameter, major diameter, aspect ratio and circularity were obtained. Spheroid volume (V) was calculated according to the formula $V = [(a^2)x(b)]/2$, in which a and b represent the minor and major diameter,

respectively. For the growth profile characterization, images of 128 spheroids per condition have been collected at each time point.

2.4.2. Spheroid dissociation and single cell counting

To assess the number of cells per spheroid over time, six-to-eight MCTS were harvested using a p5000 pipette to preserve their integrity, and then pooled in a microtube. Culture medium was carefully removed and spheroids were washed with 200 µL of phosphate buffered saline (PBS, Sigma Aldrich, France). After addition of 50 µL of trypsin (Sigma Aldrich, France), samples were incubated at 37 °C for 30 minutes and pipetted every 5 minutes with a p200 pipette to facilitate the dissociation of spheroids into a single-cell suspension. The enzyme action was stopped by the addition of 50 µL of FBS-containing culture medium. The total cell number per sample was measured using the Countess II Automated Cell Counter (Thermo Fisher Scientific, France) and the average cell number per spheroid was calculated dividing it by the number of used spheroids. Experiments have been performed in triplicate.

2.4.3. Adenosine Triphosphate (ATP) cell viability assay

Individual MCTS (n=6) were harvested from the round bottom wells and transferred in a microtube using a p5000 pipette. Culture medium was carefully removed, spheroids were washed with PBS (200 µL) to remove any extracellular ATP and then redispersed in 50 µL of phenol red-free DMEM. The spheroid suspension (50 µL) was then transferred into white-opaque 96-well plates (Corning®, Sigma Aldrich, France) and 50 µL of CellTiter-Glo® 3D reagent (Promega, France) was added into each well. Plates were protected from light and gently shaken for 10 minutes (room temperature) to induce spheroid lysis. Samples were incubated for additional 20 minutes in the dark, at room-temperature, to stabilize the bioluminescent signal, which was then recorded using a benchtop plate reader (EnSpire Alpha

2390; Perkin-Elmer, USA). The ATP concentration in each sample was quantified by using a calibration curve based on rATP standards (Promega, France) according to the manufacturer instructions.

Assessment of cell viability after exposure to doxorubicin was carried out according to the same protocol with a slight modification. Briefly, spheroids were cultured in 96 round-bottom well plates in 200 µL of medium. At determined time points, 150 µL of medium was carefully removed and 50 µL of CellTiter-Glo® 3D Reagent was added to each well (total final volume 100 µL). Plates were gently shaken in the dark for 10 minutes to lyse the samples and incubated for additional 20 minutes at room-temperature to stabilize the bioluminescent signal. Then, samples were individually transferred into white-opaque 96-well plates and the signal was measured using a benchtop plate reader (EnSpire Alpha 2390; Perkin-Elmer, USA) (8 replicates per condition, n=2).

2.4.4. In vitro luciferase assay

The bioluminescence signal produced by luciferase-expressing PANC-1 or BxPC-3 cells was measured using the Neolite Reporter Gene Assay System (Perkin-Elmer, France) according to manufacturer instructions. Briefly, spheroids were cultured in 96 round-bottom well plates in 200 µL of medium. At determined time points, 150 µL of medium was carefully removed and 50 µL of Neolite reagent was added to each well (total final volume 100 µL). Plates were protected from light and gently shaken for 10 minutes (room temperature) to induce spheroid lysis. Samples were incubated for additional 20 minutes in the dark at room-temperature to stabilize the bioluminescent signal. Samples (100 µL) were individually transferred into white-opaque 96-well plates and the signal was measured using a benchtop plate reader (EnSpire Alpha 2390; Perkin-Elmer, USA) (6 or 8 replicates per condition, at least n=3).

In another set of experiments, samples (100 µL) were individually transferred to a black-opaque 96-well plate (Corning®, Sigma Aldrich, France) and plate images were acquired using the IVIS Lumina® LT Series III (PerkinElmer, USA) (at least 3 replicates per condition, n=3). Images were processed using the Living Image software (PerkinElmer, USA).

2.4.5. Histology and immunohistochemistry

MCTS were fixed for 2 hours in 500 µL of 4% paraformaldehyde (Roti®-Histofix 4%, Roth Sochiel EURL, France) at room temperature. After inclusion in 4% low-melting agarose (Thermo Fisher Scientific, France), spheroids were embedded in paraffin and sectioned (Plate-Forme HistIM, Institut Cochin, Paris France). Sections (5 µm) were stained with haematoxylin and eosin (H&E) according to standard protocols. For immunohistochemical staining, the heat-mediated antigen retrieval of antibodies was carried out in citrate buffer at different pH (according to manufacturer protocols) and sections (5 µm) were then incubated with monoclonal antibody to cytokeratin AE1/AE3 (mouse, dil 1:50; M351501-2 Dako, France), fibronectin (rabbit, dil 1:250; ab2413 Abcam, UK) or CD-31 (mouse, dil 1:20; M082301-2 Dako, France). Primary antibodies were detected with peroxidase-conjugated secondary antibodies by using diaminobenzidine (DAB) as chromogen and haematoxylin as counterstain.

2.4.6. Selective Plane Illumination Microscopy (SPIM)

4-days old fluorescently-labelled spheroids were fixed in 500 µL of 4% paraformaldehyde (Roti®-Histofix 4%) (1 h, room temperature) and then permeabilized with 500 µL of 0.1% Triton X-100 (Sigma Aldrich, France) in PBS (1 h, room temperature). Then, Triton solution was replaced with 200 µL of PBS and cell nuclei were stained overnight with Hoechst 33342 (NucBlue™ Reagent, Thermo Fisher Scientific, France) in the dark at room temperature. MCTS were imaged with the Lightsheet Z.1 Microscope (Carl Zeiss, Germany) equipped with

a Plan-Apochromat 20x 1NA water-immersion objective lens with left and right illumination. Hoechst, GFP and RFP fluorescent signals were recorded after sample excitation at 405, 488 and 561 nm, respectively. Samples were scanned using the Zen 2014 SP1 Black-Edition software (Carl Zeiss, Germany) and optical slices of 1 µm thickness were processed for the 3D reconstruction of each sample with the Image-J® software.

2.4.7. MCTS embedding in fibrin matrix

PANC 1:MRC-5:HUVEC (ratio 1:9:4, LbL, VEGF) spheroids were prepared by using RFP-expressing HUVEC cells and cultured for 4 days before the embedding in a fibrin matrix. Individual MCTS were harvested from the round bottom wells and transferred in a microtube using a p5000 pipette. Culture medium was carefully removed and spheroids were redispersed in 250 µL of bovine fibrinogen (Sigma Aldrich, France) solution (2.5 $mg.mL^{-1}$) in PBS with aprotinin (0.15 U. mL^{-1} Sigma Aldrich, France) and type I collagen (0.2 $mg.mL^{-1}$, Gibco, France) [44]. After addition of 2.5 µL of thrombin (final concentration 0.5 U/ml, Sigma, France), single spheroids were transferred into the wells of a Lab-Tek®II Chamber SlideTM (Thermo Fisher Scientific, France). The chamber slide was placed at room temperature for 5 minutes to allow fibrin polymerization and then 400 µL of EGM-2 medium was added. Embedded MCTS were maintained in a humid atmosphere at 37 °C with 5% CO_2 for three days before to perform confocal imaging. Samples were imaged with an inverted Leica TCS SP8 microscope gated-STED (Leica, Germany) using a HC PL Fluotar CS2 10x/0.30 dry objective lens. The instrument was equipped with a WLL Laser (587 nm excitation wavelength for RFP). Red fluorescence emission was collected with a 597-800 nm wide emission slits. Transmission images were acquired with the same laser line and a PMT-trans detector. The pinhole was set at 1.0 Airy unit giving 4.29 µm optical slice thickness. 12 bit numerical images were done with Leica SP8 LAS X software (Version 2.0.1; Leica, Germany).

2.4.8. Cytotoxicity evaluation

PANC-1 or BxPC-3 (seeding density 500 cells/well) spheroids (indicated as MCTS_#1 and MCTS_#1_{BxPC-3}, respectively) and PANC-1:MRC-5:HUVEC or BxPC-3:MRC-5:HUVEC (ratio 1:9:4, LbL, VEGF) spheroids (indicated as MCTS_#3 and MCTS_#3_{BxPC-3}, respectively) were prepared and cultured for 4 days before treatment with a series of concentrations of drugs (doxorubicin (doxo) and gemcitabine (gem)) in culture medium. At the end of the incubation period (48 h and/or 72 h), cytotoxicity assessment was performed by *(i)* optical imaging *(see 2.4.1)*; *(ii)* ATP quantification *(see 2.4.3)* and/or *(iii)* qualitative and quantitative measurements of the bioluminescent signal *(see 2.4.4)*. Untreated spheroids were used as control. The viability was calculated according to the ratio of the signal of the well containing treated spheroids *versus* the average signal of control wells (*i.e.*, untreated spheroids).

2.4.9. Statistical analysis

Data are presented as mean values with standard error of mean (s.e.m). Statistical analysis was performed with the Prism GraphPad 7.0 software and the significance was calculated using a two-way Anova method, with a Sidak's multiple comparison post-test in which $p < 0.05$ was considered statistically significant (*$p < 0.05$, **$p < 0.005$, *** $p < 0.0005$, **** $p < 0.0001$).

3. Results and discussion

3.1. Construction and characterization of multicellular tumor spheroids

Mono-type multicellular tumor spheroids

MCTS consisting of cancer cells only have been constructed according to the liquid overlay technique. We have used the PANC-1 cell line, reported as aggressive and poorly differentiated [45, 46], and whose capacity to form multicellular spheroids had been previously described [47-53]. However, to our knowledge no comprehensive characterization of the growth profile of these spheroids was available. Hence, we have prepared PANC-1 spheroids by seeding cancer cells in non-adherent poly-HEMA-coated round-bottom plates at different densities (corresponding to 500, 1000, 2500 and 5000 cells per well) and carried out a broad analysis. Optical imaging at day 4 post seeding revealed the formation of uniform and reproducible 3D structures, whose volume, ATP content and cell number have been monitored over time for a period of 17 days. Representative images of spheroids made with 500 cells (Fig. 1a), showed the spontaneous assembly of cancer cells in compact spheroids with only few surrounding scattered isolated cells (day 4). Spheroid size increased over time and a dark central region was observed at days 13 and 17 post seeding. Similar behaviour was observed for spheroids prepared by seeding higher cell numbers (Fig. S1).

The follow up of the spheroid volume clearly revealed a variation rate inversely proportional to the number of seeded cells per well (Fig. 1b). The lowest cell density (500 cells/well) resulted in the formation of spheroids characterized by the fastest proliferation rate with the major diameter that rapidly increased from 400-500 μm (day 4) to 800-900 μm (day 17), corresponding to a 10-times increase of the volume (from 0.03 to 0.3 mm^3). On the contrary, only a 2-fold increase was observed for spheroids prepared by seeding 5000 cells/well.

The number of cells per spheroid, representative of the proliferation capacity of PANC-1 cell in 3D conditions, followed a similar profile (Fig. 1c). Seeding of 500 and 5000 cells/well led to

spheroids containing at day 4, an average of 2000 (increment by a factor of 4) and 14000 cells (increment by a factor of 2.7), respectively. The delayed proliferation of spheroids prepared at the highest cells density was also confirmed by a less rapid variation of the ATP content over time (Fig. 1d).

On the basis of these results, we have chosen for further studies spheroids made by seeding 500 cells/well. These spheroids will be from now indicated as MCTS_#1. Histological analysis of these spheroids by H&E and cytokeratin staining, at day 4 from seeding, revealed a uniform cell distribution and a compact core in which cells tightly adhered to each other (Fig. 1e, f). However, MCTS_#1 did not stain for fibronectin (Fig. 1g), clearly revealing the lack of deposition of this ECM component. The histological analysis at day 17 post seeding was in agreement with these results and no fibronectin staining was detectable (Fig. S2). According to the upregulation of FN in PDAC stroma and its crucial involvement in cancer cells survival, invasion and drug resistance [54-56], it was evident that these spheroids made of PANC-1 cells only did not allow to appropriately mimic the *in vivo* complexity of the PDAC.

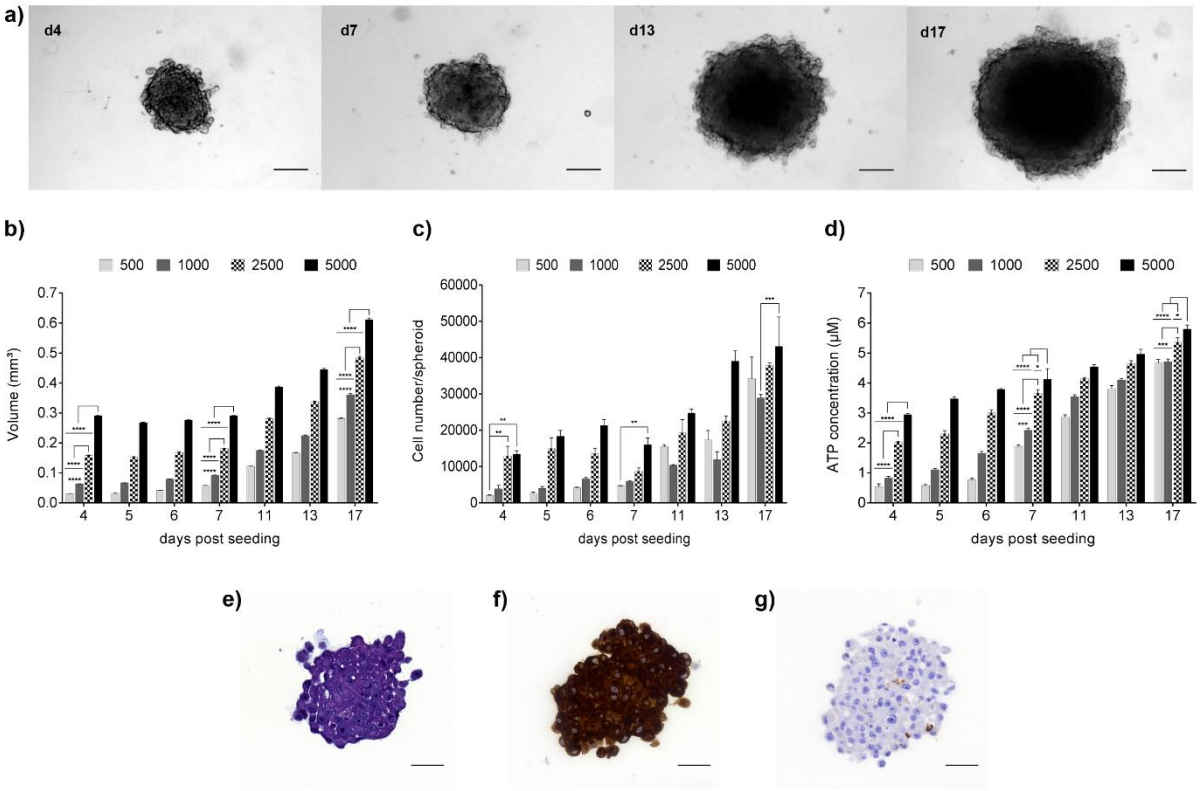

Fig. 1. Mono-type PANC-1 spheroid characterization. (a) Representative optical imaging of MCTS_#1 (seeding density of 500 cells per well) at days 4, 7, 13 and 17 post seeding. Scale bars: 200 µm. Evolution over time of (b) volume, (c) cell number and (d) ATP content per spheroid as function of the initial seeding density. Values represent mean ± s.e.m. *$p < 0.05$ **$p < 0.005$, *** $p < 0.0005$ **** $p < 0.0001$ by a two-way Anova method, with a Sidak's post-test at days 4, 7 and 17 post seeding, chosen as representative time points. Histological analysis of 5 µm sections of MCTS_#1 at day 4 post seeding: (e) haematoxylin eosin staining, (f) cytokeratin AE1/AE3 and (g) fibronectin immunostaining. Scale bars: 50 µm.

Hetero-type multicellular spheroids: co-culture of cancer cells and fibroblasts

To mimic the tumor-stroma interactions we further gradually increased the complexity of our model and we moved to the construction of an intermediate hetero-type MCTS consisting of cancer cells and fibroblasts. We used MRC-5 fibroblasts, previously reported as a valid alternative to pancreatic stromal cells thanks to their capacity to promote the invasive phenotype of pancreatic cancer cells and to modulate the expression of cell adhesion markers as efficiently

as PDAC patient-derived fibroblasts and pancreatic stellate cells [57, 58]. Noteworthy is that this cell line has already been used in different multicellular pancreatic tumor models and it offered the possibility to study the tumor microenvironment and investigate the cross-talk between cancer cells and stromal ones [40, 59-61]. In addition, successful reconstruction of the interaction between cancer cells and the microenvironment using fibroblasts derived from healthy tissues has also been described for breast cancer 3D models [37, 62, 63].

By keeping constant the number of PANC-1 (*i.e.,* 500 cells per spheroid at day 0), we investigated co-cultures with fibroblasts at different ratios (1:1, 1:2, 1:4 and 1:9). In all tested conditions the two cell types spontaneously self-assembled without the need of supporting material and the size of spheroids progressively increased over time (from day 4 to day 17) (Fig. 2a, b and Fig S3). Whatever the tested ratio, the number of cells per spheroid at day 4 was lower than expected according to the seeding density, thus clearly showing that a loss of cells occurred during the first steps of the co-culture assembly (Fig. 2c). Nevertheless, once formed, all spheroids continued to grow regularly as also confirmed by the evolution of the volume and the ATP content (Fig. 2b, d). Note that co-culture with fibroblasts enhanced the metabolic activity of cancer cells compared to spheroids made of PANC-1 only, resulting in a comparable effect to that induced by primary tumor-associated fibroblasts in Transwell® co-cultures [35]. The ratio PANC-1:MRC-5 1:9, which allowed, at day 4, to construct spheroids with the highest cell number was selected for further studies. These spheroids will be from now indicated as MCTS_#2.

H&E staining at day 4 of MCTS_#2 showed the assembly of the two cell types and the predominant localization in the core of elongated cells surrounded by a population of round cells (Fig. 2e). The latter was positively stained for the cytokeratin AE1/AE3 marker (specific for the detection of epithelial cells of neoplastic origin) thus revealing the peripheral localization of the PANC-1 cells. On the contrary, the core was characterized by

cytokeratin-negative cells and was positively stained for the fibronectin, thus suggesting the accumulation in this area of fibroblasts responsible for the secretion of the ECM component (Fig. 2f, g).

Nevertheless, at day 7 post seeding (Fig. 2h-l) all cells positively stained for the cytokeratin marker revealing the infiltration of cancer cells in the core of the spheroid previously filled by fibroblasts. The disappearance of the MRC-5 cells well correlated with the negligible fibronectin staining (Fig. 2i, l). Same results were obtained at day 17 post seeding. (Fig. S4)

Cell spatial distribution at day 4 was assessed also by Selective Plane Illumination Microscopy (SPIM) imaging of MCTS_#2 constructed using GFP-expressing MRC-5 fibroblasts (Fig. S5a-c). SPIM allowed to observe the spheroid mass in the whole and to collect high resolution images, bypassing the limitations in terms of depth of laser penetration of traditional imaging methods such as the confocal microscopy [64-66]. The blue staining of nuclei (Hoechst 33342) showed the distribution of cells in the 3D structure (Fig. S5b) and the green fluorescence in the core confirmed the presence of fibroblasts in this region at day 4 post seeding (Fig. S5c). However, in agreement with the histological characterization, at day 7 post seeding (Fig. S5d-f), the reduction of the green signal indicated the progressive loss of fibroblasts and their gradual replacement by rapidly proliferating cancer cells (Fig. S5f).

These results showed that the tumor microenvironment was not static and a progressive transformation occurred over time leading to the integration of cancer cells and components of the microenvironment (*i.e.*, fibroblasts and fibronectin) for up to 4 days. A progressive loss of fibroblasts had been previously observed in lung [67] and prostate [68] MCTS as well as in spheroid co-cultures of fibroblasts and endothelial cells. [69, 70] However, to the best of our knowledge, this is the first time that modifications of the composition of long-term cultured MCTS have been precisely assessed by histological and microscopic analysis in a hetero-type pancreatic tumor model.

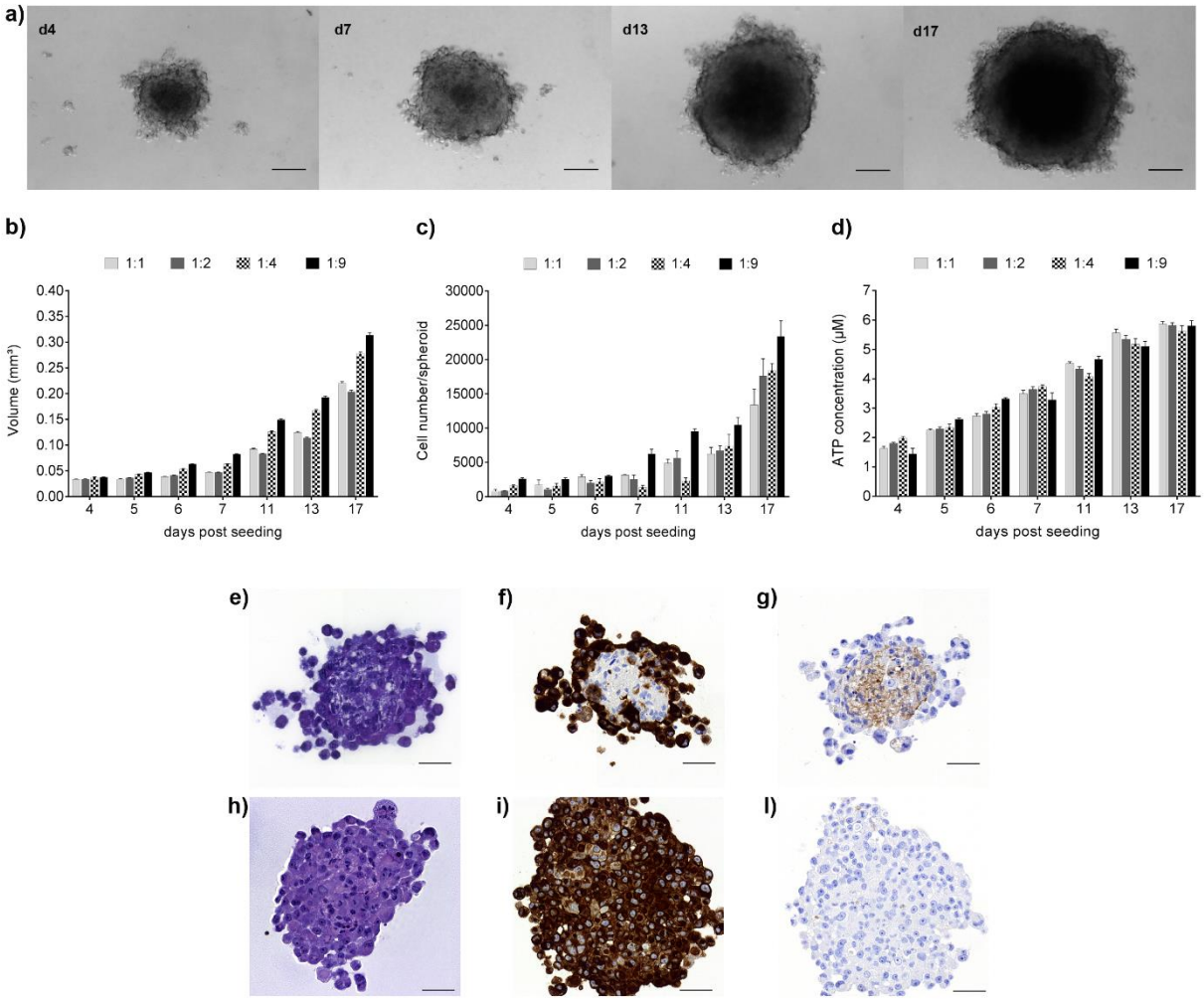

Fig. 2. Hetero-type PANC-1: MRC-5 spheroid characterization. (a) Representative optical imaging of MCTS_#2 (PANC-1:MRC-5 seeding ratio 1:9) at days 4, 7, 13 and 17 post seeding. Scale bars: 200 µm. Evolution over time of (b) volume, (c) cell number and (d) ATP content per spheroid as function of the initial seeding density (PANC-1:MRC-5 ratio 1:1, 1:2, 1:4 and 1:9). Values represent mean ± s.e.m. Histological analysis of 5 µm sections of MCTS_#2 at day 4 (e, f, g) and day 7 (h, i, l) post seeding: (e, h) haematoxylin eosin staining, (f, i) cytokeratin AE1/AE3 and (g, l) fibronectin immunostaining. Scale bars: 50 µm.

Hetero-type multicellular spheroids: triple co-culture of cancer cells, fibroblasts and endothelial cells

The last step in the construction of a new model consisted in the introduction of HUVEC endothelial cells and the establishment of a triple co-culture. Note that hetero-type pancreatic tumor spheroids including fibroblast and endothelial components have not been previously reported. The choice of the HUVEC has been driven by their large availability and stable features compared to tumor-derived endothelial cells, whose wide application in routine in vitro studies is still hindered by several obstacles. They include, for instance, the scarce availability of fresh tumor sample, the difficulty to isolate tumor endothelial cells with high degree of purity, the lack of well-defined culture conditions with consequent phenotype mutation, their short life span and thus the possibility to use them for a limited number of passages only [71].

Firstly, PANC-1 cancer cells (500 cells per spheroid at day 0) were mixed with MRC-5 fibroblasts and HUVEC at 1:9:4 ratio and seeded on poly-HEMA-coated plates according to the liquid overlay technique already used for MCTS_#1 and MCTS_#2. Cell assembly and spatial organization of the three cellular components were regularly monitored as early as 2 days after seeding. Also in this case, immunostaining revealed a peripheral localization of the cytokeratin-positive cells (*i.e.*, PANC-1 cells) while the cytokeratin-negative ones and fibronectin were localised in the core of the spheroid (Fig. S6a, b). However, this assembly was characterized by weak hetero-type cell-to-cell contacts as attested by the frequent loss of PANC-1 cells during sample preparation. In addition, CD31 immunostaining, used as a marker of the endothelial cells, highlighted only a feeble presence of HUVEC cells (Fig. S6c); MCTS_#1 and MCTS_#2 spheroids at day 4 post seeding were used as negative controls (Fig. S7). Two days after (day 4), spheroids were more compact (Fig. S6d-f) but the CD31 staining was negligible (Fig. S6f). As we evidenced above, a reorganisation of the cell composition with

time was observed also in these spheroids, with a progressive accumulation of PANC-1 cells in the core of the spheroids together with a decrease of the fibronectin content (Fig. S6d, e).

To promote integration and residence of endothelial cells within the spheroid, the preparation method was slightly modified. Briefly, before mixing with PANC-1 and HUVEC, a Layer-by-Layer (LbL) nanofilm of fibronectin and gelatin (FN-G) was constructed at the surface of the MRC-5 fibroblasts, according to a previously validated technique [72]. The FN-G coating on the cell membrane, which mimicked the natural ECM [73-75], had already been successfully applied to the construction of stable multilayer multicellular tissues on Transwell® inserts [43, 76-80]. Such coating was capable of promoting cell adhesion into the spheroids, facilitating the triple co-culture with the HUVEC cells. Compared to the traditional protocol, this approach allowed to increase the number of CD31-positive cells, which after two days of culture formed a discontinuous layer at the fibroblasts/cancer cells interface. However, the latter were only loosely attached to the external spheroid boundaries (Fig. S8a-c). At day 4, spheroids were more compact, but also in this case the presence of endothelial cells was strongly reduced (Fig. S8d-f). As expected, the FN-G nanofilm supported a better assembly of the three cell types in the spheroid, but it was not enough to ensure their prolonged 3D co-culture. Of note, because of the presence of the adhesive FN-G layer, these spheroids were less fragile and could be more easily handled, thus facilitating their routinely use at day 4. Accordingly, this preparation method was maintained for all the successive experiences. Although collagen, rather than gelatin, is the main component of the pancreatic tumor ECM, the latter has been chosen for the cell coating due to its solubility in neutral medium, which ensures a higher cytocompatibility. On the contrary, the acidic solution of collagen is not well suitable for the culture condition due to the low pH value. Moreover, being the gelatin obtained by collagen denaturation, it maintains a chemical composition very similar to that of the parent molecule.

Significant improvement was then obtained by culturing the LbL-assembled spheroids in medium supplemented with VEGF (50 ng.mL^{-1}), a well-known endothelial survival factor [81] and angiogenesis inducer [82]. In addition, VEGF already showed a beneficial effect on the viability and sprouting of HUVEC spheroids [34, 83, 84]. In these experimental conditions, at day 2, a thick layer of endothelial cells was observed around the fibronectin-rich cytokeratin-negative core (Fig. S9c). On the contrary, no stable adhesion of cancer cells occurred, and they could be easily lost during sample preparation (Fig. S9). A more compact spheroid was, instead, obtained after a culture period of 4 days (Fig. 3a). PANC-1 cancer cells, that are cytokeratin-positive cells, mostly organized in an external layer surrounding cytokeratin-negative cells with which cell-to-cell hetero contacts were established (Fig. 3b). Fibronectin staining revealed the homogenous distribution of this ECM protein in the core (Fig. 3c) in which a network of CD31-positive endothelial cells was also well visible (Fig. 3d). The latter closely resembled to the collapsed vessels observed in PDAC [31, 33]. Thus, after opportune optimization of the experimental conditions (*that is*, LbL coating and VEGF supplement) we successfully constructed a hetero-type pancreatic MCTS based on a triple co-culture of cancer cells, fibroblasts and endothelial cells. These spheroids (PANC-1:MRC-5:HUVEC, LbL, VEGF) will be from now indicated as MCTS_#3.

Histological analysis showed that the optimal triple co-culture was achieved at day 4. At day 7, all cells were positively stained for the cytokeratin (Fig. 4a), as previously observed also for MCTS_#2 (Fig. 2h-l), and no more fibronectin and HUVEC were detectable (Fig. 4b, c).

The spatial distribution of the three cell types at day 4 was assessed in detail by SPIM imaging of MCTS_#3 constructed using GFP-expressing MRC-5 fibroblasts and RFP-expressing HUVEC cells (Fig. 5). The uniform blue staining revealed a homogeneous distribution of cells in the 3D structure (Fig. 5b). The green fluorescence confirmed the presence of fibroblasts in the core (Fig. 5c), which correlated with histology images showing a core made of cytokeratin-

negative cells and rich in fibronectin (Fig. 3b, c). Red-fluorescent HUVECs were also visible in the centre of the spheroid confirming their strong association with the fibroblasts (Fig. 5d). The slightly elongated shape of HUVEC suggested their potential capacity, in opportune conditions to develop vessel-like networks (Fig S10), as previously observed by Boutin and co-workers in their imaging analysis of rat cortical spheroids [85].

In agreement with the histological characterization, SPIM imaging of MCTS_#3 spheroids at day 7 showed the progressive loss of the stromal cells. (Fig. 5e-h).

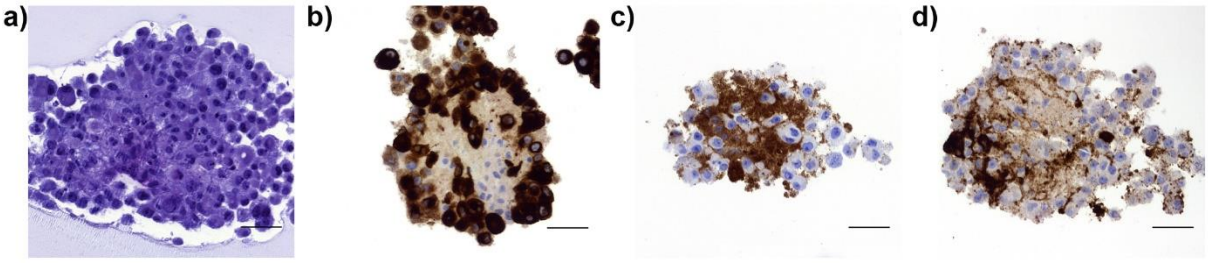

Fig. 3. Hetero-type PANC-1:MRC-5:HUVEC spheroid characterization. Histological analysis of 5 µm sections of MCTS_#3 (PANC-1:MRC-5:HUVEC, LbL, VEGF) at day 4 post seeding: (a) haematoxylin eosin staining, (b) cytokeratin AE1/AE3, (c) fibronectin and (d) CD31 immunostaining. Scale bars: 50 µm.

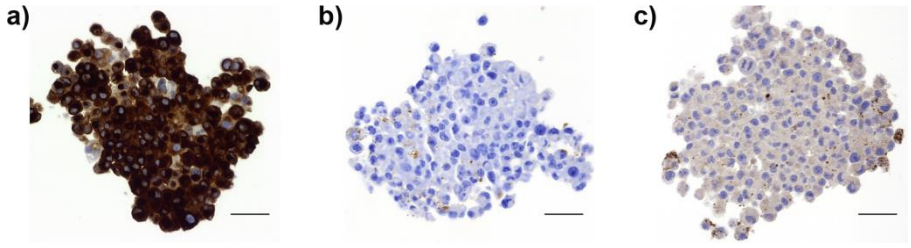

Fig. 4. Hetero-type PANC-1:MRC-5:HUVEC spheroid characterization. Histological analysis of 5 µm sections of hetero-type PANC-1:MRC-5:HUVEC MCTS_#3 (ratio 1:9:4) at day 7 post seeding: (a) cytokeratin AE1/AE3, (b) fibronectin and (c) CD31 immunostaining. Scale bars: 50 µm.

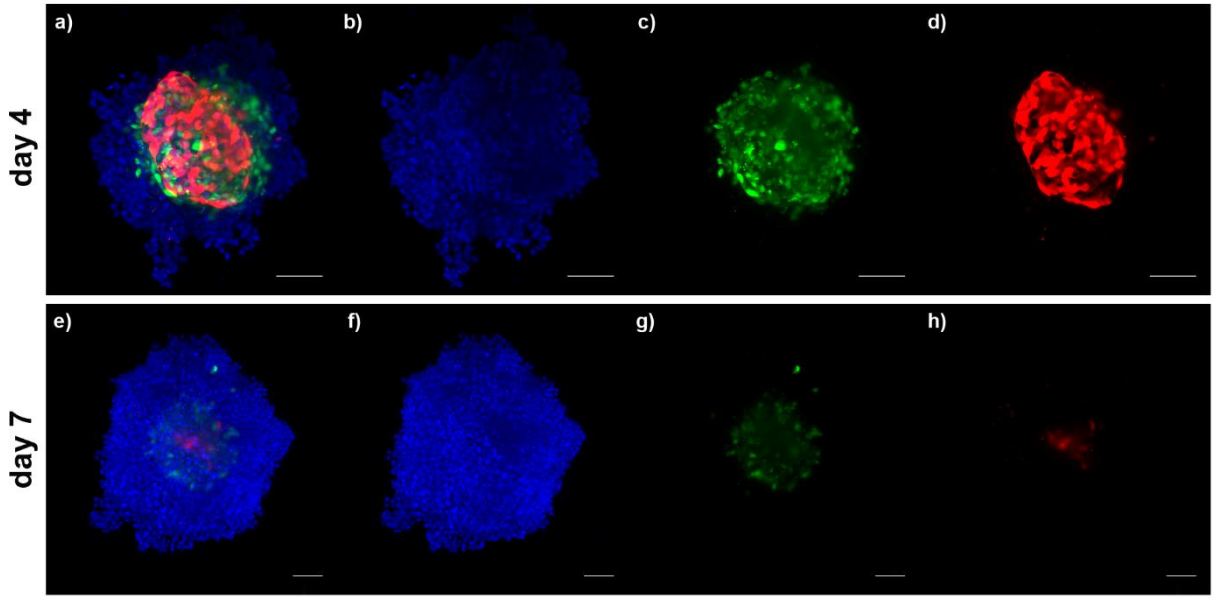

Fig. 5. SPIM 3D topography of MCTS_#3 (PANC-1:MRC-5:HUVEC, LbL, VEGF) at day 4 and day 7. (a, e) Overlay of blue (Hoechst 33342, nuclei), green (GFP-expressing MRC-5 fibroblasts) and red (RFP-expressing HUVECs) fluorescence; (b, f) single blue channel (Excitation/emission 405/440 nm) showing all cell nuclei; (c, g) single green channel (Excitation/emission 488/525 nm) showing GFP-expressing MRC-5 fibroblasts; (d, h) single red channel (Excitation/emission 561/605 nm) with RFP-expressing HUVEC cells. Scale bars: 100 µm.

According to the stability of the triple co-culture, characterization of MCTS_#3 was carried out for up to 7 days from seeding. Morphology and growth kinetic were microscopically assessed and optical-images showed spheroids with a dense core and a ruffled peripheral cell layer whose compactness increased over time (Fig. 6a). Since day 2, the triple co-culture led to the formation of larger spheroids as compared to MCTS_#1 and MCTS_#2 (Fig. S11) and they reached a mean volume of 0.09 mm^3 (~ 600 µm in diameter) at day 4 (Fig. 6b). At this time point, MCTS_#1 and MCTS_#2 showed a mean volume of 0.03 and 0.04 mm^3, respectively (Fig. 1 and 2). Variation of the number of cells over time revealed the same trend (Fig. 6c). Also in this case, single cell counting in MCTS_#3 evidenced that not all cells assembled to form the spheroids but that a certain loss occurred, and the number of cells per spheroid at day 2 was lower than the seeded one. This corroborated the hypothesis of the existence of a critical initial

number of cells for establishing heterotypic interactions and stable 3D assembly. The strong influence of the microenvironment on the spheroid metabolic activity was confirmed by the ATP content (Fig. 6d) which, at day 4, was up to two times higher than in spheroids made of only cancer cells (0.54 and 1.2 µM for MCTS_#1 and MCTS_#3). This influence, likely mediated by the direct 3D cell-to-cell contact as well as by the production of growth factors and cytokines [60, 86] persisted also at day 7 when spheroids where mainly composed of cancer cells (Fig. 4). Among the secreted soluble factors, the hepatocyte growth factor (HGF) might play a key role. It has been demonstrated that by binding to its transmembrane receptor c-Met, the HGF may activate several signaling pathways involved in pancreatic cancer cells growth and invasion, tumor progression, desmoplastic reaction and resistance to treatment [87-89]. In addition, previous studies have reported a high secretion of HGF by MRC-5 fibroblasts, which was responsible of an enhanced proliferation and migration of several types of cancer cells [35, 90-92]. Thus, although further investigation would be required to confirm this hypothesis, it is possible that the proliferation of PANC-1 might be mediated by the HGF secreted by the MRC-5 cells. Overall, these results demonstrated that the structural and functional interactions between cancer cells and several stromal components have been successfully recreated in MCTS_#3.

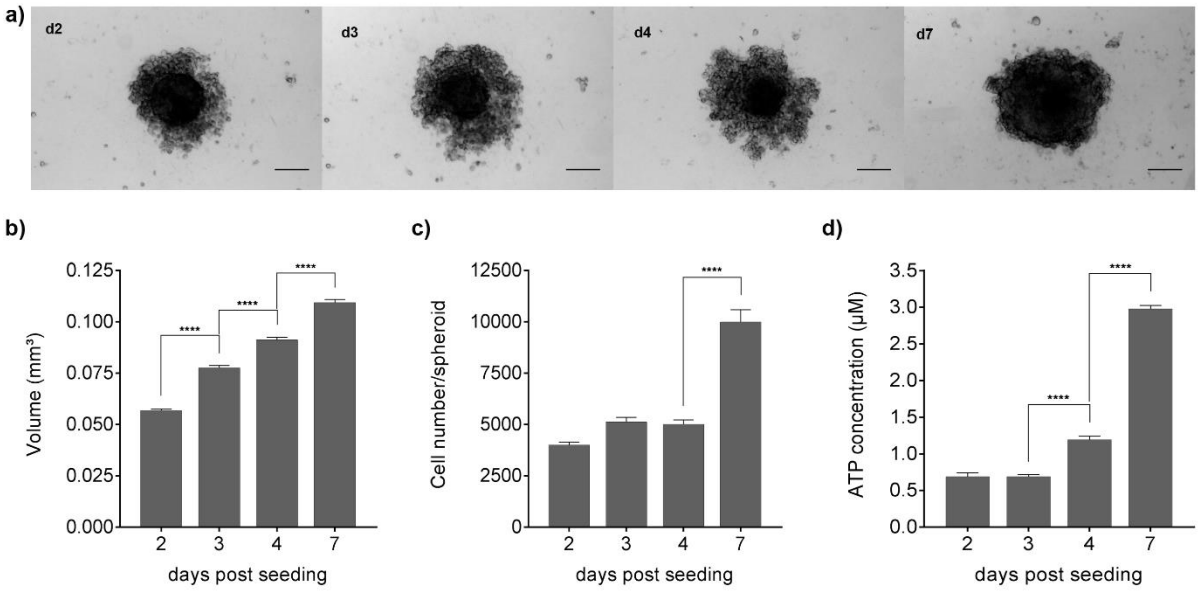

Fig. 6. Hetero-type PANC-1:MRC-5:HUVEC spheroid characterization. (a) Representative optical imaging of MCTS_#3 (PANC-1:MRC-5:HUVEC, LbL, VEGF) at days 2, 3, 4 and 7 post seeding. Scale bars: 200 µm. Evolution over time of (b) volume, (c) cell number and (d) ATP content per spheroid in MCTS_#3. Values represent mean ± s.e.m. **** $p < 0.0001$ by a two-way Anova method, with a Sidak's post-test.

3.2. Cytotoxic studies: effect of the tumor microenvironment

It is well known that the tumor microenvironment strongly influences the drug sensitivity of cancer cells and may affect the efficacy of treatments [29]. Therefore, we aimed to verify whether the MCTS_#3 model was capable or not to reproduce such influence. Firstly, as proof of concept we assessed the cell viability in MCTS_#3 and MCTS_#1 after a 48 h and 72 h exposure to a single dose of doxorubicin (0.5 µM, IC_{50} for PANC-1 cells grown in 2D monolayer). Because of their stability and 3D compact structure, spheroids at day 4 were used for the onset of the treatment. Spheroids were constructed using luciferase-expressing PANC-1 cells, enabling to specifically monitor the cytotoxicity of doxorubicin on cancer cells by quantification of the luciferase activity. After 48 h of incubation, the survival of cancer cells

was similar in both types of spheroids and only a general decrease of ~10% could be measured in comparison to their respective untreated controls (Fig. 7a). However, after longer exposure (72 h) higher survival was observed in MCTS_#3. Sensitivity of cancer cells was influenced by the presence of the tumor microenvironment (Fig. 7a). Bioluminescence images of these spheroids were in agreement with the quantitative results. Only a weak difference of the pseudocolor was observed between control (untreated) and doxo-treated MCTS_#3. On the contrary, for MCTS_#1 the colour changed from green to light blue (lowest values) after treatment which underlined the higher sensitivity to doxorubicin (Fig. 7b). Accordingly, the overall spheroid viability, as measured by the ATP content, was also significantly different at 72 h and confirmed the key role of the tumor microenvironment on the sensitivity of the spheroids to the treatment (Fig. 7c). In addition, the anti-proliferative effect of the drug has been also microscopically assessed by collecting bright-field images of spheroids (n=64 per condition). Quantitative information of the growth inhibition was provided by the variation of the spheroid volume after treatment [93]. Once again data revealed the lowest anticancer efficacy of the drug on MCTS_#3 and further corroborated the influence of the microenvironment on the proliferation of the tumor mass (Fig. 6d). The higher sensitivity of MCTS_#1 compared to MCTS_#3 was observed also after exposure of spheroids, constructed using luciferase-expressing PANC-1 cells, to a series of doxorubicin concentrations (Fig. S12a). Similar results were obtained after incubation with gemcitabine, in spite of the different mechanism of actions of the two anticancer drugs (Fig. S12b). Indeed, doxorubicin exerts its cytotoxic activity by intercalation between DNA base pairs blocking DNA replication and transcription, blockade of topoisomerase II activity as well as generation of free radicals, [94] while, on the other hand, gemcitabine acts as nucleoside analogue [95].

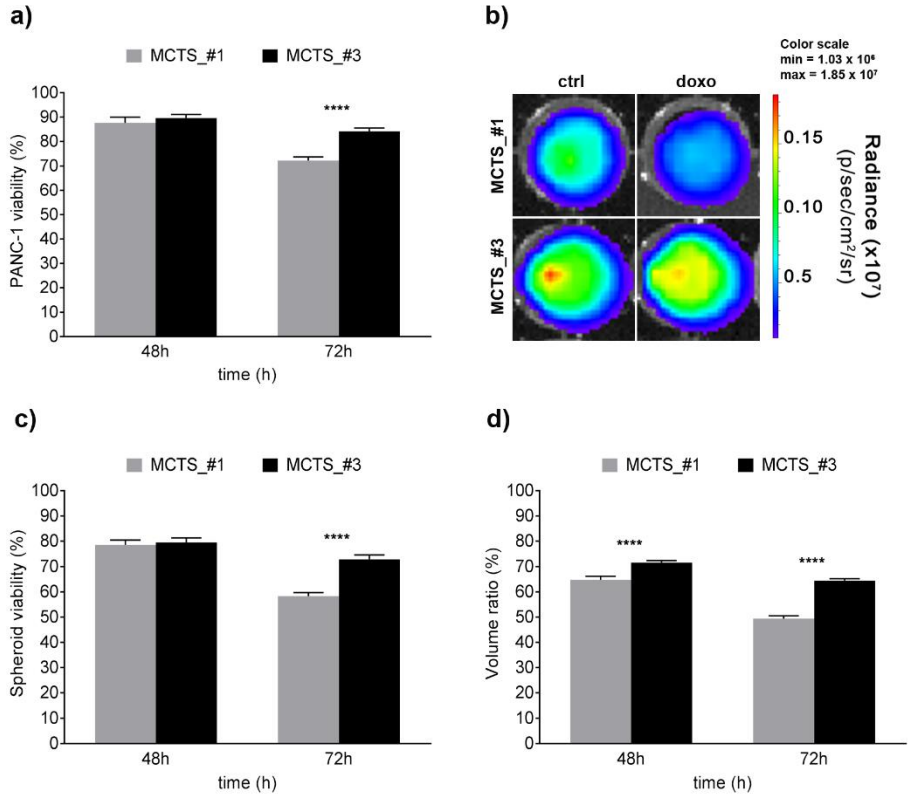

Fig. 7. (a) PANC-1 cell viability (luciferase activity) in MCTS_#1 and MCTS_#3 following exposure to doxorubicin (0.5 µM) for 48 h and 72 h (n=3). Spheroids have been constructed using luciferase-expressing PANC-1 cells. (b) Representative bioluminescence images of control and doxo-treated MCTS_#1 and MCTS_#3. Incubation time 72 h. (c) Spheroid viability (ATP quantification) following exposure to doxorubicin (0.5 µM) for 48 h and 72 h (n=2). (d) Spheroid growth inhibition (volume measurement) following exposure to doxorubicin (0.5 µM) for 48 h and 72 h. Data represents mean ± s.e.m. **** $p < 0.0001$ by a two-way Anova method, with a Sidak's post-test.

Noteworthy is that after exposure to doxorubicin and gemcitabine, MCTS_#3 displayed higher resistance to treatments also when compared to MCTS_#2, thus confirming the crucial role of a complex tumor microenvironment consisting of multiple cell types (Fig. S13).

We have then modified the culture condition to assess whether similar results could be obtained by using another pancreatic cell line. Thus, both mono-type and hetero-type (i.e., triple co-culture) multicellular spheroids, have been constructed replacing the PANC-1 cell line with the

BxPC-3 one (indicated as MCTS_#1$_{BxPC-3}$ and MCTS_#3$_{BxPC-3,}$ respectively). However, exposure of these spheroids to growing concentrations of doxorubicin and gemcitabine did not induce a dose/effect response. In addition, for each concentration tested, we observed a higher viability of mono-type spheroids compared to the hetero-type triple co-culture (Fig. S14). This was attributed to the more compact structure of MCTS_#1$_{BxPC-3}$ (Fig. S15), which artefactually opposed to the diffusion/penetration of the drug through the tumor mass. These results clearly highlight that accurate selection of the cell types used for the construction of the spheroids and characterization of the resulting cell assembly are a key requisite to develop valuable tools for accurate preclinical screening of therapeutic strategies for pancreatic cancer treatment.

4. Conclusions

The failure of treatments and the poor prognosis of pancreatic ductal adenocarcinoma are related to the extremely complex physio-pathology of this tumor, combining abundant fibrosis and collapsed vasculature, which strongly limits drugs accessibility. In this study, we reported on the construction and detailed characterization of a scaffold-free 3D model capable to integrate in a hetero-type multicellular spheroid the cancerous component of the pancreatic tumor as well as its microenvironment made of fibroblasts, endothelial cells and extracellular matrix. To our knowledge, no analogous model combining the fibrotic tissue and a collapsed vessel-like structure, both hallmark of the PDAC, has been previously constructed. Evaluation of spheroid growth and response to treatment confirmed the influence of the microenvironment on drug sensitivity of pancreatic cancer cells, and showed the capacity of this model to replicate the resistance to treatments often observed *in vivo.* Overall, we believe that this easy to handle spheroid model, reproducing crucial features of the PDAC, could find application in standardized drug screening protocols as well as in the assessment of cancer cells-stroma interactions and tumor angiogenesis.

Acknowledgements

The research leading these results has received funding from the European Union's HORIZON 2020 Programme for research, technological development and demonstration under grant agreement no. 642028 H2020-MSCA-ITN-2014.The CNRS and the French Ministry of Research are also warmly acknowledged for financial support. Pr Christian Poüs and Mr Patrick Lêchene are gratefully acknowledged for the creation of the image-processing macro with Image-J®. Miss Meriem Garfa-Traoré and Mr Nicolas Goudin of the Cell Imaging Platform (SFR Neker, Paris France) are warmly acknowledged for the technical assistance and the fruitful discussions on the result interpretation during the imaging with SPIM. Dr Stéphanie Denis is gratefully acknowledged for the assistance in cell lines maintenance. Dr Delphine Courilleau, technical manager of the CIBLOT Plate-Forme (Institut Paris-Saclay d'Innovation Thérapeutique, Châtenay Malabry France), is warmly acknowledged for the assistance with the bioluminescence measurements. Miss Maryline Favier and Miss Fabiola Ely-Marius from HistIM Plate-Forme (Institut Cochin, Paris France) are warmly acknowledged for their expertise in the histological analysis of spheroid samples. Pr Andras Dinnyes, Dr Julianna Kobolak and Dr Anita Fehér from BioTalentum Ltd (Gödöllő, Hungary) are gratefully acknowledged for the technical assistance in the lentiviral transduction of the cell lines.

Conflict of interest

The authors declare no conflict of interest.

References

[1] M.J. Bissell, D. Radisky, Putting tumours in context, Nat. Rev. Cancer 1(1) (2001) 46–54.

[2] K. Moriya, E. Bae, K. Honda, K. Sakai, T. Sakaguchi, I. Tsujimoto, H. Kamisoyama, D.R. Keene, T. Sasaki, T. Sakai, A fibronectin-independent mechanism of collagen fibrillogenesis in adult liver remodeling, Gastroenterology 140(5) (2011) 1653–1663.

[3] K.E. Kadler, A. Hill, E.G. Canty-Laird, Collagen fibrillogenesis: fibronectin, integrins, and minor collagens as organizers and nucleators, Curr. Opin. Cell Biol. 20(5-24) (2008) 495–501.

[4] U. Yaqoob, S. Cao, U. Shergill, K. Jagavelu, Z. Geng, M. Yin, T.M. de Assuncao, Y. Cao, A. Szabolcs, S. Thorgeirsson, M. Schwartz, J.D. Yang, R. Ehman, L. Roberts, D. Mukhopadhyay, V.H. Shah, Neuropilin-1 stimulates tumor growth by increasing fibronectin fibril assembly in the tumor microenvironment, Cancer Res. 72(16) (2012) 4047–4059.

[5] E. Serres, F. Debarbieux, F. Stanchi, L. Maggiorella, D. Grall, L. Turchi, F. Burel-Vandenbos, D. Figarella-Branger, T. Virolle, G. Rougon, E. Van Obberghen-Schilling, Fibronectin expression in glioblastomas promotes cell cohesion, collective invasion of basement membrane in vitro and orthotopic tumor growth in mice, Oncogene 33(26) (2014) 3451–3462.

[6] O. Pontiggia, R. Sampayo, D. Raffo, A. Motter, R. Xu, M.J. Bissell, E.B.d.K. Joffé, M. Simian, The tumor microenvironment modulates tamoxifen resistance in breast cancer: a role for soluble stromal factors and fibronectin through β1 integrin, Breast Cancer Res. and treatment 133(2) (2012) 459–471.

[7] Nakagawa, Nakayama, Nagata, Yoshida, Kawahara, Hirosue, Tanaka, Yuno, Matsuoka, Kojima, Yoshitake, Hiraki, Shinohara, Overexpression of fibronectin confers cell adhesionmediated drug resistance (CAM-DR) against 5-FU in oral squamous cell carcinoma cells, Int. J. Oncol. 44(4) (2014) 1376–1384.

[8] M.J. Bissell, W.C. Hines, Why don't we get more cancer? A proposed role of the microenvironment in restraining cancer progression, Nat. Med. 17 (2011) 320–329.

[9] C. Feig, A. Gopinathan, A. Neesse, D.S. Chan, N. Cook, D.A. Tuveson, The pancreas cancer microenvironment, Clin. Cancer Res. 18(16) (2012) 4266–4276.

[10] D. Mahadevan, D.D. Von Hoff, Tumor-stroma interactions in pancreatic ductal adenocarcinoma, Mol. Cancer Ther. 6(4) (2007) 1186–1197.

[11] C. Choe, Y.-S. Shin, S.-H. Kim, M.-J. Jeon, S.-J. Choi, J. Lee, J. Kim, Tumor–stromal Interactions with Direct Cell Contacts Enhance Motility of Non-small Cell Lung Cancer Cells Through the Hedgehog Signaling Pathway, Anticancer Res. 33(9) (2013) 3715–3723.

[12] C. Gaggioli, S. Hooper, C. Hidalgo-Carcedo, R. Grosse, J.F. Marshall, K. Harrington, E. Sahai, Fibroblast-led collective invasion of carcinoma cells with differing roles for RhoGTPases in leading and following cells, Nat. Cell Biol. 9(12) (2007) 1392–1400.

[13] R. Kalluri, M. Zeisberg, Fibroblasts in cancer, Nat. Rev. Cancer 6(5) (2006) 392–401.

[14] D. von Ahrens, T.D. Bhagat, D. Nagrath, A. Maitra, A. Verma, The role of stromal cancer-associated fibroblasts in pancreatic cancer, J. Hematol. Oncol. 10 (2017) 76–83.

[15] P. Carmeliet, R.K. Jain, Angiogenesis in cancer and other diseases, Nature 407(6801) (2000) 249–257.

[16] J.W. Franses, A.B. Baker, V.C. Chitalia, E.R. Edelman, Stromal Endothelial Cells Directly Influence Cancer Progression, Sci. Transl. Med. 3(66) (2011) 5–13.

[17] G. Lazzari, P. Couvreur, S. Mura, Multicellular tumor spheroids: a relevant 3D model for the in vitro preclinical investigation of polymer nanomedicines, Polym. Chem. 8(34) (2017) 4947–4969.

[18] G. Mehta, A.Y. Hsiao, M. Ingram, G.D. Luker, S. Takayama, Opportunities and challenges for use of tumor spheroids as models to test drug delivery and efficacy, J. Control. Release 164(2) (2012) 192–204.

[19] E.C. Costa, A.F. Moreira, D. de Melo-Diogo, V.M. Gaspar, M.P. Carvalho, I.J. Correia, 3D tumor spheroids: an overview on the tools and techniques used for their analysis, Biotechnol. Adv. 34(8) (2016) 1427–1441.

[20] P. Benien, A. Swami, 3D tumor models: history, advances and future perspectives, Future Oncol. 10(7) (2014) 1311–1327.

[21] X. Cui, Y. Hartanto, H. Zhang, Advances in multicellular spheroids formation, J. R. Soc. Interface 14(127) (2017).

[22] E. Fennema, N. Rivron, J. Rouwkema, C. van Blitterswijk, J. de Boer, Spheroid culture as a tool for creating 3D complex tissues, Trends Biotechnol. 31(2) (2013) 108–115.

[23] C.R. Thoma, M. Zimmermann, I. Agarkova, J.M. Kelm, W. Krek, 3D cell culture systems modeling tumor growth determinants in cancer target discovery, Adv. Drug Deliver. Rev. 69–70(Supplement C) (2014) 29–41.

[24] A.-L. Bulin, M. Broekgaarden, T. Hasan, Comprehensive high-throughput image analysis for therapeutic efficacy of architecturally complex heterotypic organoids, Sci. Rep. 7(1) (2017) 16645–16656.

[25] E.L.S. Fong, D.A. Harrington, M.C. Farach-Carson, H. Yu, Heralding a new paradigm in 3D tumor modeling, Biomaterials 108(Supplement C) (2016) 197–213.

[26] L. Gu, D.J. Mooney, Biomaterials and emerging anticancer therapeutics: engineering the microenvironment, Nat. Rev. Cancer 16(1) (2016) 56–66.

[27] K.M. Tevis, Y.L. Colson, M.W. Grinstaff, Embedded Spheroids as Models of the Cancer Microenvironment, Adv. Biosyst. 1(10) (2017) 1700083–1700099.

[28] D.W. Infanger, M.E. Lynch, C. Fischbach, Engineered Culture Models for Studies of Tumor-Microenvironment Interactions, Ann. Rev. Biomed. Eng. 15(1) (2013) 29–53.

[29] A. Adamska, A. Domenichini, M. Falasca, Pancreatic Ductal Adenocarcinoma: Current and Evolving Therapies, Int. J. Mol. Sci. 18(7) (2017) 1338–1380.

[30] S. Pandol, M. Edderkaoui, I. Gukovsky, A. Lugea, A. Gukovskaya, Desmoplasia of Pancreatic Ductal Adenocarcinoma, Clin. Gastroenterol. Hepatol. 7(11 0) (2009) S44–S47.

[31] V. Longo, O. Brunetti, A. Gnoni, S. Cascinu, G. Gasparini, V. Lorusso, D. Ribatti, N. Silvestris, Angiogenesis in pancreatic ductal adenocarcinoma: A controversial issue, Oncotarget 7(36) (2016) 58649–58658.

[32] H.-x. Zhan, B. Zhou, Y.-g. Cheng, J.-w. Xu, L. Wang, G.-y. Zhang, S.-y. Hu, Crosstalk between stromal cells and cancer cells in pancreatic cancer: New insights into stromal biology, Cancer Lett. 392(Supplement C) (2017) 83–93.

[33] M. Korc, Pathways for aberrant angiogenesis in pancreatic cancer, Mol. Cancer 2(1) (2003) 8–15.

[34] B.M. Beckermann, G. Kallifatidis, A. Groth, D. Frommhold, A. Apel, J. Mattern, A.V. Salnikov, G. Moldenhauer, W. Wagner, A. Diehlmann, R. Saffrich, M. Schubert, A.D. Ho, N. Giese, M.W. Büchler, H. Friess, P. Büchler, I. Herr, VEGF expression by mesenchymal stem cells contributes to angiogenesis in pancreatic carcinoma, Brit. J. Cancer 99(4) (2008) 622–631.

[35] M. Majety, L.P. Pradel, M. Gies, C.H. Ries, Fibroblasts Influence Survival and Therapeutic Response in a 3D Co-Culture Model, PloS One 10(6) (2015) e0127948.

[36] M.J. Ware, V. Keshishian, J.J. Law, J.C. Ho, C.A. Favela, P. Rees, B. Smith, S. Mohammad, R.F. Hwang, K. Rajapakshe, C. Coarfa, S. Huang, D.P. Edwards, S.J. Corr, B. Godin, S.A. Curley, Generation of an in vitro 3D PDAC stroma rich spheroid model, Biomaterials 108(Supplement C) (2016) 129–142.

[37] D.L. Priwitaningrum, J.-B.G. Blondé, A. Sridhar, J. van Baarlen, W.E. Hennink, G. Storm, S. Le Gac, J. Prakash, Tumor stroma-containing 3D spheroid arrays: A tool to study nanoparticle penetration, J. Control. Release 244(Part B) (2016) 257–268.

[38] V. Brancato, V. Comunanza, G. Imparato, D. Corà, F. Urciuolo, A. Noghero, F. Bussolino, P.A. Netti, Bioengineered tumoral microtissues recapitulate desmoplastic reaction of pancreatic cancer, Acta Biomater. 49(Supplement C) (2017) 152–166.

[39] H. Shoval, A. Karsch-Bluman, Y. Brill-Karniely, T. Stern, G. Zamir, A. Hubert, O. Benny, Tumor cells and their crosstalk with endothelial cells in 3D spheroids, Sci. Rep. 7(1) (2017) 10428–10438.

[40] J. Kuen, D. Darowski, T. Kluge, M. Majety, Pancreatic cancer cell/fibroblast co-culture induces M2 like macrophages that influence therapeutic response in a 3D model, PloS One 12(7) (2017) e0182039.

[41] P. Noel, R. Muñoz, G.W. Rogers, A. Neilson, D.D. Von Hoff, H. Han, Preparation and Metabolic Assay of 3-dimensional Spheroid Co-cultures of Pancreatic Cancer Cells and Fibroblasts, J. Vis. Exp. (126) (2017) 56081–56088.

[42] J. Carlsson, J.M. Yuhas, Liquid-overlay culture of cellular spheroids, Recent Results Cancer Res. 95 (1984) 1–23.

[43] M. Matsusaki, D. Hikimoto, A. Nishiguchi, K. Kadowaki, K. Ohura, T. Imai, M. Akashi, 3D-fibroblast tissues constructed by a cell-coat technology enhance tight-junction formation of human colon epithelial cells, Biochem. Bioph. Res. Co. 457(3) (2015) 363–369.

[44] S. Kim, H. Lee, M. Chung, N.L. Jeon, Engineering of functional, perfusable 3D microvascular networks on a chip, Lab Chip 13(8) (2013) 1489–1500.

[45] M. Lieber, J. Mazzetta, W. Nelson-Rees, M. Kaplan, G. Todaro, Establishment of a continuous tumor-cell line (PANC-1) from a human carcinoma of the exocrine pancreas, Int. J. Cancer 15(5) (1975) 741–747.

[46] E.L. Deer, J. González-Hernández, J.D. Coursen, J.E. Shea, J. Ngatia, C.L. Scaife, M.A. Firpo, S.J. Mulvihill, Phenotype and genotype of pancreatic cancer cell lines, Pancreas 39(4) (2010) 425–435.

[47] B. Sipos, S. Möser, H. Kalthoff, V. Török, M. Löhr, G. Klöppel, A comprehensive characterization of pancreatic ductal carcinoma cell lines: towards the establishment of an in vitro research platform, Virchows Arch. 442(5) (2003) 444–452.

[48] Z. Wen, Q. Liao, Y. Hu, L. You, L. Zhou, Y. Zhao, A spheroid-based 3-D culture model for pancreatic cancer drug testing, using the acid phosphatase assay, Braz. J. Med. Biol. Res. 46(7) (2013) 634–642.

[49] E.J. McLeod, A.D. Beischer, J.S. Hill, A.H. Kaye, Multicellular Tumor Spheroids Grown from Pancreatic Carcinoma Cell Lines: Use as an Orthotopic Xenograft in Athymic Nude Mice, Pancreas 14(3) (1997) 237–248.

[50] M. Beer, N. Kuppalu, M. Stefanini, H. Becker, I. Schulz, S. Manoli, J. Schuette, C. Schmees, A. Casazza, M. Stelzle, A. Arcangeli, A novel microfluidic 3D platform for culturing pancreatic ductal adenocarcinoma cells: comparison with in vitro cultures and in vivo xenografts, Sci. Rep. 7 (2017) 1325–1336.

[51] P. Longati, X. Jia, J. Eimer, A. Wagman, M.-R. Witt, S. Rehnmark, C. Verbeke, R. Toftgård, M. Löhr, R.L. Heuchel, 3D pancreatic carcinoma spheroids induce a matrix-rich, chemoresistant phenotype offering a better model for drug testing, BMC Cancer 13(1) (2013) 95–107.

[52] S.-E. Yeon, D.Y. No, S.-H. Lee, S.W. Nam, I.-H. Oh, J. Lee, H.-J. Kuh, Application of Concave Microwells to Pancreatic Tumor Spheroids Enabling Anticancer Drug Evaluation in a Clinically Relevant Drug Resistance Model, PloS One 8(9) (2013) e73345.

[53] M.J. Ware, K. Colbert, V. Keshishian, J. Ho, S.J. Corr, S.A. Curley, B. Godin, Generation of Homogenous Three-Dimensional Pancreatic Cancer Cell Spheroids Using an Improved Hanging Drop Technique, Tissue Eng. Part C Methods 22(4) (2016) 312–321.

[54] M. Topalovski, R.A. Brekken, Matrix control of pancreatic cancer: New insights into fibronectin signaling, Cancer Lett. 381(1) (2016) 252–258.

[55] S. Jagadeeshan, Y.R. Krishnamoorthy, M. Singhal, A. Subramanian, J. Mavuluri, A. Lakshmi, A. Roshini, G. Baskar, M. Ravi, L.D. Joseph, K. Sadasivan, A. Krishnan, A.S. Nair, G. Venkatraman, S.K. Rayala, Transcriptional regulation of fibronectin by p21-activated kinase-1 modulates pancreatic tumorigenesis, Oncogene 34(4) (2015) 455–464.

[56] E.C. Vaquero, M. Edderkaoui, K.J. Nam, I. Gukovsky, S.J. Pandol, A.S. Gukovskaya, Extracellular matrix proteins protect pancreatic cancer cells from death via mitochondrial and nonmitochondrial pathways, Gastroenterology 125(4) 1188–1202.

[57] K. Ohuchida, K. Mizumoto, M. Murakami, L.-W. Qian, N. Sato, E. Nagai, K. Matsumoto, T. Nakamura, M. Tanaka, Radiation to Stromal Fibroblasts Increases Invasiveness of Pancreatic Cancer Cells through Tumor-Stromal Interactions, Cancer Res. 64(9) (2004) 3215–3222.

[58] F.E.M. Froeling, T.A. Mirza, R.M. Feakins, A. Seedhar, G. Elia, I.R. Hart, H.M. Kocher, Organotypic Culture Model of Pancreatic Cancer Demonstrates that Stromal Cells Modulate E-Cadherin, β-Catenin, and Ezrin Expression in Tumor Cells, Am. J. Pathol. 175(2) (2009) 636–648.

[59] D.P. Jones, W. Hanna, G.M. Cramer, J.P. Celli, In situ measurement of ECM rheology and microheterogeneity in embedded and overlaid 3D pancreatic tumor stroma co-cultures via passive particle tracking, J. Innov. Opt. Health Sci. 10(06) (2017) 1742003–1742011.

[60] H. Fujita, K. Ohuchida, K. Mizumoto, T. Egami, K. Miyoshi, T. Moriyama, L. Cui, J. Yu, M. Zhao, T. Manabe, M. Tanaka, Tumor–stromal interactions with direct cell contacts enhance proliferation of human pancreatic carcinoma cells, Cancer Sci. 100(12) (2009) 2309–2317.

[61] Z. Lao, C.J. Kelly, X.-Y. Yang, W.T. Jenkins, E. Toorens, T. Ganguly, S.M. Evans, C.J. Koch, Improved Methods to Generate Spheroid Cultures from Tumor Cells, Tumor Cells & Fibroblasts or Tumor-Fragments: Microenvironment, Microvesicles and MiRNA, PloS One 10(7) (2015) e0133895.

[62] P. Correa de Sampaio, D. Auslaender, D. Krubasik, A.V. Failla, J.N. Skepper, G. Murphy, W.R. English, A heterogeneous in vitro three dimensional model of tumour-stroma interactions regulating sprouting angiogenesis, PloS One 7(2) (2012) e30753.

[63] C. Mazio, C. Casale, G. Imparato, F. Urciuolo, P.A. Netti, Recapitulating spatiotemporal tumor heterogeneity in vitro through engineered breast cancer microtissues, Acta Biomater. (2018) https://doi.org/10.1016/j.actbio.2018.04.028.

[64] F. Pampaloni, N. Ansari, E.H.K. Stelzer, High-resolution deep imaging of live cellular spheroids with light-sheet-based fluorescence microscopy, Cell Tissue Res. 352(1) (2013) 161–177.

[65] C. Lorenzo, C. Frongia, R. Jorand, J. Fehrenbach, P. Weiss, A. Maandhui, G. Gay, B. Ducommun, V. Lobjois, Live cell division dynamics monitoring in 3D large spheroid tumor models using light sheet microscopy, Cell Div. 6(1) (2011) 22–29.

[66] Q. Fu, B.L. Martin, D.Q. Matus, L. Gao, Imaging multicellular specimens with real-time optimized tiling light-sheet selective plane illumination microscopy, Nat. Commun. 7 (2016) 11088–11097.

[67] A. Amann, M. Zwierzina, G. Gamerith, M. Bitsche, J.M. Huber, G.F. Vogel, M. Blumer, S. Koeck, E.J. Pechriggl, J.M. Kelm, W. Hilbe, H. Zwierzina, Development of an Innovative 3D Cell Culture System to Study Tumour - Stroma Interactions in Non-Small Cell Lung Cancer Cells, PloS One 9(3) (2014) e92511.

[68] T. Eder, A. Weber, H. Neuwirt, G. Grunbacher, C. Ploner, H. Klocker, N. Sampson, I.E. Eder, Cancer-Associated Fibroblasts Modify the Response of Prostate Cancer Cells to Androgen and Anti-Androgens in Three-Dimensional Spheroid Culture, Int. J. Mol. Sci. 17(9) (2016) 1458–1472;

[69] L.A. Kunz-Schughart, J.A. Schroeder, M. Wondrak, F. van Rey, K. Lehle, F. Hofstaedter, D.N. Wheatley, Potential of fibroblasts to regulate the formation of three-dimensional vessel-

like structures from endothelial cells in vitro, American journal of physiology. Am. J. Physiol. Cell Physiol. 290(5) (2006) C1385–1398.

[70] C.W. Eckermann, K. Lehle, S.A. Schmid, D.N. Wheatley, L.A. Kunz-Schughart, Characterization and modulation of fibroblast/endothelial cell co-cultures for the in vitro preformation of three-dimensional tubular networks, Cell Biol. Int. 35(11) (2011) 1097–1110.

[71] A.C. Dudley, Tumor Endothelial Cells, Cold Spring Harb. Perspect. Med. 2(3) (2012) a006536–a006554.

[72] M. Matsusaki, K. Kadowaki, Y. Nakahara, M. Akashi, Fabrication of Cellular Multilayers with Nanometer-Sized Extracellular Matrix Films, Angew. Chem. Int. Ed. 46(25) (2007) 4689–4692.

[73] S. Johansson, G. Svineng, K. Wennerberg, A. Armulik, L. Lohikangas, Fibronectin-integrin interactions, Front. Biosci. 2(1997) 126–146.

[74] J. Labat-Robert, Cell–Matrix interactions, the role of fibronectin and integrins. A survey, Pathol. Biol. 60(1) (2012) 15–19.

[75] A.J. Zollinger, M.L. Smith, Fibronectin, the extracellular glue, Matrix Biol. 60(Supplement C) (2017) 27–37.

[76] A. Nishiguchi, H. Yoshida, M. Matsusaki, M. Akashi, Rapid Construction of Three-Dimensional Multilayered Tissues with Endothelial Tube Networks by the Cell-Accumulation Technique, Adv. Mater. 23(31) (2011) 3506–3510.

[77] K. Kadowaki, M. Matsusaki, M. Akashi, Three-dimensional constructs induce high cellular activity: Structural stability and the specific production of proteins and cytokines, Biochem. Biophys. Res. Commun. 402(1) (2010) 153–157.

[78] H. Hosoya, K. Kadowaki, M. Matsusaki, H. Cabral, H. Nishihara, H. Ijichi, K. Koike, K. Kataoka, K. Miyazono, M. Akashi, M.R. Kano, Engineering fibrotic tissue in pancreatic cancer:

A novel three-dimensional model to investigate nanoparticle delivery, Biochem. Biophys. Res. Commun. 419(1) (2012) 32–37.

[79] A. Nishiguchi, M. Matsusaki, Y. Asano, H. Shimoda, M. Akashi, Effects of angiogenic factors and 3D-microenvironments on vascularization within sandwich cultures, Biomaterials 35(17) (2014) 4739–4748.

[80] A. Matsuzawa, M. Matsusaki, M. Akashi, Construction of three-dimensional liver tissue models by cell accumulation technique and maintaining their metabolic functions for long-term culture without medium change, J. Biomed. Mater. Res. A 103(4) (2015) 1554–1564.

[81] T. Alon, I. Hemo, A. Itin, J. Pe'er, J. Stone, E. Keshet, Vascular endothelial growth factor acts as a survival factor for newly formed retinal vessels and has implications for retinopathy of prematurity, Nat. Med. 1(10) (1995) 1024–1028.

[82] G. Bergers, L.E. Benjamin, Tumorigenesis and the angiogenic switch, Nat. Rev. Cancer 3(6) (2003) 401–410.

[83] T. Korff, S. Kimmina, G. Martiny-Baron, H.G. Augustin, Blood vessel maturation in a 3-dimensional spheroidal coculture model: direct contact with smooth muscle cells regulates endothelial cell quiescence and abrogates VEGF responsiveness, FASEB J. 15(2) (2001) 447–457.

[84] T. Korff, H.G. Augustin, Integration of Endothelial Cells in Multicellular Spheroids Prevents Apoptosis and Induces Differentiation, J. Cell Biol. 143(5) (1998) 1341–1352.

[85] M.E. Boutin, L.L. Kramer, L.L. Livi, T. Brown, C. Moore, D. Hoffman-Kim, A three-dimensional neural spheroid model for capillary-like network formation, J. Neurosci. Methods 299 (2017) 55–63.

[86] R.F. Hwang, T. Moore, T. Arumugam, V. Ramachandran, K.D. Amos, A. Rivera, B. Ji, D.B. Evans, C.D. Logsdon, Cancer-Associated Stromal Fibroblasts Promote Pancreatic Tumor Progression, Cancer Res. 68(3) (2008) 918–926.

[87] S.P. Pothula, Z. Xu, D. Goldstein, A.V. Biankin, R.C. Pirola, J.S. Wilson, M.V. Apte, Hepatocyte growth factor inhibition: a novel therapeutic approach in pancreatic cancer, Br. J. Cancer. 114 (2016) 269–280.

[88] S.P. Pothula, Z. Xu, D. Goldstein, N. Merrett, R.C. Pirola, J.S. Wilson, M.V. Apte, Targeting the HGF/c-MET pathway: stromal remodelling in pancreatic cancer, Oncotarget 8(44) (2017) 76722–76739.

[89] W. Rizwani, A.E. Allen, J.G. Trevino, Hepatocyte Growth Factor from a Clinical Perspective: A Pancreatic Cancer Challenge, Cancer 7(3) (2015) 1785–1805.

[90] N. Kanaji, M. Yokohira, Y. Nakano-Narusawa, N. Watanabe, K. Imaida, N. Kadowaki, S. Bandoh, Hepatocyte growth factor produced in lung fibroblasts enhances non-small cell lung cancer cell survival and tumor progression, Resp. Res. 18(1) (2017) 118–127.

[91] Y. Kitajima, T. Ide, T. Ohtsuka, K. Miyazaki, Induction of hepatocyte growth factor activator gene expression under hypoxia activates the hepatocyte growth factor/c-Met system via hypoxia inducible factor-1 in pancreatic cancer, Cancer Sci. 99(7) (2008) 1341–1347.

[92] Q. Li, W. Wang, T. Yamada, K. Matsumoto, K. Sakai, Y. Bando, H. Uehara, Y. Nishioka, S. Sone, S. Iwakiri, K. Itoi, T. Utsugi, K. Yasumoto, S. Yano, Pleural Mesothelioma Instigates Tumor-Associated Fibroblasts To Promote Progression via a Malignant Cytokine Network, Am. J. Pathol. 179(3) (2011) 1483–1493.

[93] J. Friedrich, C. Seidel, R. Ebner, L.A. Kunz-Schughart, Spheroid-based drug screen: considerations and practical approach, Nat. Protocols 4(3) (2009) 309–324.

[94] C.F. Thorn, C. Oshiro, S. Marsh, T. Hernandez-Boussard, H. McLeod, T.E. Klein, R.B. Altman, Doxorubicin pathways: pharmacodynamics and adverse effects, Pharmacogenet. Genom. 21(7) (2011) 440–446.

[95] L.H. Reddy, P. Couvreur, Novel approaches to deliver gemcitabine to cancers, Curr. Pharm. Design 14(11) (2008) 11243–11247.